

Photoinduced valley-dependent equal-spin Andreev reflection in Ising superconductor junction

Wei-Tao Lu(卢伟涛), Yue Mao(毛岳), and Qing-Feng Sun(孙庆丰)
Citation: Chin. Phys. B, 2023, 32 (**10**): 107403. DOI: 10.1088/1674-1056/aceee6
Journal homepage: http://cpb.iphy.ac.cn; http://iopscience.iop.org/cpb

What follows is a list of articles you may be interested in

Strain-modulated anisotropic Andreev reflection in a graphene-based superconducting junction

Xingfei Zhou(周兴飞), Ziming Xu (许子铭), Deliang Cao(曹德亮), and Fenghua Qi(戚凤华)
Chin. Phys. B, 2022, 31 (**11**): 117403. DOI: 10.1088/1674-1056/ac7553

Asymmetric Fraunhofer pattern in Josephson junctions from heterodimensional superlattice V_5S_8

Juewen Fan(范珏雯), Bingyan Jiang(江丙炎), Jiaji Zhao(赵嘉佶), Ran Bi(毕然), Jiadong Zhou(周家东), Zheng Liu(刘政), Guang Yang(杨光), Jie Shen(沈洁), Fanming Qu(屈凡明), Li Lu(吕力), Ning Kang(康宁), and Xiaosong Wu(吴孝松)
Chin. Phys. B, 2022, 31 (**5**): 057402. DOI: 10.1088/1674-1056/ac5d30

Dynamic vortex Mott transition in triangular superconducting arrays

Zi-Xi Pei(裴子玺), Wei-Gui Guo(郭伟贵), and Xiang-Gang Qiu(邱祥冈)
Chin. Phys. B, 2022, 31 (**3**): 037404. DOI: 10.1088/1674-1056/ac3cb1

Electronic properties and interfacial coupling in Pb islands on single-crystalline graphene

Jing-Peng Song(宋靖鹏) and Ang Li(李昂)
Chin. Phys. B, 2022, 31 (**3**): 037401. DOI: 10.1088/1674-1056/ac1b8e

Anomalous Josephson current in quantum anomalous Hall insulator-based superconducting junctions with a domain wall structure

Qing Yan(闫青), Yan-Feng Zhou(周彦峰), Qing-Feng Sun(孙庆丰)
Chin. Phys. B, 2020, 29 (**9**): 097401. DOI: 10.1088/1674-1056/aba272

SPECIAL TOPIC — Valleytronics

Photoinduced valley-dependent equal-spin Andreev reflection in Ising superconductor junction

Wei-Tao Lu(卢伟涛)[1,†], Yue Mao(毛岳)[2], and Qing-Feng Sun(孙庆丰)[2,3,‡]

[1] *School of Sciences, Nantong University, Nantong* 226019, *China*
[2] *International Center for Quantum Materials, School of Physics, Peking University, Beijing* 100871, *China*
[3] *Hefei National Laboratory, Hefei* 230088, *China*

(Received 13 June 2023; revised manuscript received 7 August 2023; accepted manuscript online 10 August 2023)

The Ising spin–orbit coupling could give rise to the spin-triplet Cooper pairs and equal-spin Andreev reflection (AR) in Ising superconductors. Here we theoretically study the valley-dependent equal-spin AR in a ferromagnet/Ising superconductor junction with a circularly polarized light applied to the ferromagnet. Because of the spin-triplet Cooper pairs and the optical irradiation, eight kinds of AR processes appear in the junction, including equal-spin AR and normal AR, the strengths and properties of which strongly depend on the valley degree of freedom. The AR probabilities for the incident electron from the two valleys exhibit certain symmetry with respect to the magnetization angle and the effective energy of light. The equal-spin AR and normal AR present different features and resonant behaviors near the superconducting gap edges. Due to equal-spin-triplet Cooper pairs, not only charge supercurrent but also spin supercurrent can transport in the Ising superconductors. The differential spin conductance for electron injecting from the two valleys can be controlled by the circularly polarized light.

Keywords: valleytronics, equal-spin Andreev reflection, spin-triplet Cooper pairs, Ising superconductor junction

PACS: 71.70.Ej, 74.45.+c, 72.25.–b **DOI:** 10.1088/1674-1056/aceee6

1. Introduction

Recently, valleytronics have attracted much attention in two-dimensional layered materials such as graphene and transition metal dichalcogenides (TMDs).[1–3] Analogous to spintronics, valleytronics aim to generate, control, and detect the valley degree of freedom, which have potential applications in semiconductor technologies and quantum information. Many topics of valleytronics have been reported in recent years, including valley-polarized transport,[4] quantum valley Hall effect,[5–7] spin–valley locked physics,[8,9] chiral optical selection rules,[10] etc. Because of the Berry phase difference for the two valleys induced by magnetic field, the giant valley splitting and unusual valley crossing are observed in the graphene resonators.[10] The strong spin–orbit coupling (SOC) and broken inversion symmetry of TMDs give rise to a valley-dependent optical selection rule, where the right (left) circularly polarized light couples to interband transitions in the K (K') valley.[9] The transition from valley-Hall phase to anomalous Hall phase and the valley-Hall conductivity switch could occur in graphene WSe_2 heterostructures under off-resonant polarized light.[11]

Andreev reflection (AR) is a process of electron–hole conversion that occurs at the interface of a normal metal (N) and superconductor (SC).[12] The incident electron in the metal is reflected at the N/SC interface as a hole, and a Cooper pair is injected into the SC. Generally, the state of Cooper pair is spin singlet. Considering the spin and valley degrees of freedom, the Cooper pair is composed of electrons from the opposite spins in opposite valleys.[13–20] Thus, it is possible to detect the valley polarization of edge states by the AR.[13] The two electrons of a Cooper pair tunneling into SC could move in opposite directions in the bilayer graphene because they belong to different valleys and the valley-chiral modes are formed at the domain walls.[16] The spin–valley switch effect can be realized between the crossed AR and the elastic cotunneling by adjusting the electric field in the antiferromagnet/SC junctions.[17]

Due to the broken inversion symmetry of TMDs, the spin splitting is opposite at the two valleys and is pinned to the out-of-plane direction, so the SOC of TMDs is termed Ising SOC.[1,2] Recent experimental works reveal that the superconductivity could be realized in various TMDs.[21–25] With the application of gate voltage, MoS_2 thin films could exhibit electric field-induced superconductivity with a critical temperature 10 K.[21] Due to the Ising SOC in TMDs such as MoS_2 and $NbSe_2$, the in-plane upper critical field of the superconductor is enhanced remarkably, which exceeds the Pauli paramagnetic limit by several times.[22,23] Hence, the so-called Ising SC (ISC) provides an opportunity to study the superconducting spintronics. Interestingly, the Ising SOC gener-

†Corresponding author. E-mail: physlu@163.com
‡Corresponding author. E-mail: sunqf@pku.edu.cn

© 2023 Chinese Physical Society and IOP Publishing Ltd

ates equal-spin triplet Cooper pairs in ISC and results in a topological superconductor with Majorana zero modes.[26,27] ISC can induce a robust topological superconducting gap in InSb nanowires with a strongly enlarged topological regime due to the equal-spin Cooper pairs.[28] The spin-singlet and spin-triplet pairing correlations could be manipulated by applying an in-plane magnetic field to the ISC.[29,30] In particular, the spin-triplet AR is investigated in the conductor/ISC hybrid junctions.[31–35] The equal-spin AR in ferromagnet/ISC junctions shows a strong magnetoanisotropy with period π, which can be enhanced by single-band ISC.[31] The equal-spin AR gives rise to the switch effect of spin-triplet Josephson current and 0–π transitions in ISC Josephson junctions.[32] The equal-spin crossed AR could take place in a ferromagnet/ISC/ferromagnet junction due to the spin-triplet Cooper pairs, and it has a significant increase for half-metal ferromagnet.[34] Furthermore, the spin transport through the N/ISC junction demonstrates that ISCs also have the characteristic of spin superconductivity.[33,35] Even so, the influence of valley degree of freedom on equal-spin AR in the ISC junction still needs to be explored.

In this paper, we theoretically investigate the property of equal-spin AR in the ferromagnet/ISC (FM/ISC) junction with a circularly polarized light applied to the FM, as shown in Fig. 1(a). It is found that although the Cooper pair is valley-singlet state in the ISC, the AR is sensitive to the valley degree of freedom due to the optical irradiation. The valley-dependent equal-spin AR and normal AR happen in different regions and exhibit different behaviors. The irradiation of light destroys the symmetry of valley-dependent AR, leading to a strong magnetoanisotropy of AR with period 2π. The equal-spin-triplet Cooper pairs could give rise to a valley-dependent spin supercurrent in the ISC. The results can be understood in terms of half-metal phase, Ising superconducting phase, and the symmetry of the system.

The rest of the paper is organized as follows. In Section 2, we give the Hamiltonian of the light-irradiated FM/ISC junction and the formula for AR. The results on valley-dependent equal-spin AR and spin transport are discussed in Section 3. Finally, a summary is presented in Section 4.

2. Theoretical model and formula

We mainly study the character of equal-spin AR under the application of light, which is a powerful method to regulate electronic properties. Many intriguing phenomena are found in the optically driven nonequilibrium systems, such as light-induced superconductivity,[36,37] photo-initiated insulator–metal transition,[38] Floquet topological phases,[39,40] and light-induced anomalous Hall effect.[41] For the circularly polarized light irradiated onto the TMDs sheet, the corresponding electromagnetic potential may be represented by $\boldsymbol{A}(t) = A(\pm\sin(\Omega t), \cos(\Omega t))$, where the signs $\pm$ refer to the right/left circular polarization, Ω is the frequency of the light, and $A = E_0/\Omega$ with E_0 being the amplitude of the electric field $\boldsymbol{E}(t) = \partial \boldsymbol{A}(t)/\partial t$. The gauge potential satisfies time periodicity $\boldsymbol{A}(t+T) = \boldsymbol{A}(t)$ with $T = 2\pi/\Omega$. When the light frequency is off resonant for any electron transitions ($\hbar\Omega \gg t_j$ with the hopping energy t_j), the effect of such an off-resonant light can be described by a static effective Hamiltonian. Based on the Floquet theory,[42] the static Hamiltonian near the valleys has the form $\eta\lambda_{\rm v}$, where the valley index $\eta = \pm$is for the K and K' valleys. $\lambda_{\rm v} = (eAv_{\rm F})^2/\hbar\Omega$ is the effective energy describing the effects of the off-resonant circularly polarized light, which is positive (negative) for the right (left) circularly polarized light. In contrast with the on-resonant optical induction which can cause the photon-assisted tunneling and photon-assisted AR due to the photon absorption/emission,[43] the off-resonant light cannot generate real photon absorption/emission but can lead to the valley-dependent band structure and valley-dependent equal-spin AR. Furthermore, the off-resonant light could also induce various topological phases such as quantum spin Hall effect and quantum valley Hall effect.[11,44,45]

The low-energy electronic properties of TMDs may be well described by a minimal band model.[9,26] Considering the magnetization vector and the off-resonant circularly polarized light, the electronic states of TMDs in the vicinity of the valleys can be approximately expressed by the two-band $k\cdot p$ Hamiltonian[26]

$$H_\eta(k) = \frac{\hbar^2k^2}{2m} + \eta\lambda_{\rm s}\sigma_z + \eta\lambda_{\rm v} + \sigma\cdot\boldsymbol{M} - \mu. \tag{1}$$

Here, k denotes the wave vector relative to the valleys K and K'. $\sigma = (\sigma_x, \sigma_y, \sigma_z)$ is the Pauli matrix of the spin space, $\lambda_{\rm s}$ is the Ising SOC strength, and μ is the chemical potential. Remarkably, the light $\lambda_{\rm v}$ could lift the valley degeneracy. $\boldsymbol{M} = M(\sin\theta\cos\varphi, \sin\theta\sin\varphi, \cos\theta)$ is the magnetization vector with the exchange energy M, the polar angle θ, and the azimuthal angle φ, which could lift the spin degeneracy and break the time-reversal symmetry. Ising SOC $\lambda_{\rm s}$ has opposite directions in opposite valleys and could induce spin-triplet pairing correlations in the in-plane directions.[26] For the FM/ISC junction, we set chemical potential $\mu = \mu_{\rm ISC}$ in the ISC region and $\mu = \mu_{\rm FM}$ in the FM region. The Ising SOC strength $\lambda_{\rm s}$ is assumed to be zero in the FM region. The light and the magnetization are only applied to the FM region [see Fig. 1(a)], where the valley degeneracy and spin degeneracy are lifted. In the ISC region, only the Ising SOC exists and there is no light field and magnetization with $\lambda_{\rm v} = M = 0$. Therefore, the time-reversal symmetry still holds in the ISC region.

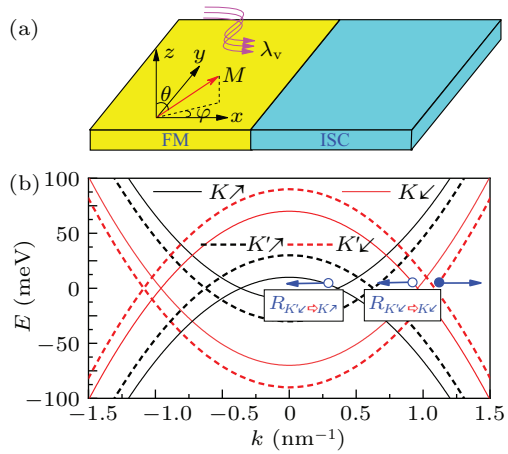


Fig. 1. (a) The schematic diagram for the FM/ISC junction. (b) The bands for different spins near the two valleys in the FM region at $\lambda_v = 10$ meV, $\mu_{FM} = 50$ meV, and $M = 30$ meV.

The Bogoliubov–de Gennes Hamiltonians for the FM/ISC junction can be written as

$$H_{BdG}(k) = \begin{pmatrix} H_\eta(k) & \hat{\Delta} \\ -\hat{\Delta}^* & -H_{\bar{\eta}}^*(-k) \end{pmatrix}, \tag{2}$$

where $\bar{\eta} = -\eta$ and $\hat{\Delta} = \Delta\, e^{i\phi} i\sigma_y$ is the s-wave superconducting order parameter with the superconducting gap Δ. The Hamiltonian $H_\eta(k)$ describes electron excitations with certain spin at certain valley, while $-H_{\bar{\eta}}^*(-k)$ describes hole excitations with opposite spin at opposite valley. The superconducting gap Δ couples the time-reversed electron and hole states from opposite spins and opposite valleys. The dispersion relations of the FM region and ISC region can be described as

$$E_{FM}^e = \frac{\hbar^2 q^2}{2m} - \mu_{FM} \pm M + \eta\lambda_v, \tag{3}$$

$$E_{FM}^h = -\frac{\hbar^2 q^2}{2m} + \mu_{FM} \pm M + \eta\lambda_v, \tag{4}$$

$$E_{ISC}^2 = \Delta^2 + \left(\frac{\hbar^2 k^2}{2m} - \mu_{ISC} \pm \lambda_s\right)^2, \tag{5}$$

where $\pm$ are for the particles with spin up and spin down, respectively. From Eqs. (3) and (4) one may find that it is half-metal phase at $\mu_{FM} < \min(M+\lambda_v, M-\lambda_v)$ and metal phase at $\mu_{FM} > \min(M+\lambda_v, M-\lambda_v)$ in the FM region. Equation (5) implies that the phase of ISC is single-band at $\mu_{ISC} < \lambda_s$ and double-band at $\mu_{ISC} > \lambda_s$. The half-metal phase and Ising superconducting phase play a key role in the AR process.

For an incident electron from the FM lead with energy E and spin s, the wave functions in the two regions of the FM/ISC junction can be written as

$$\Psi_{FM} = f_{e,s}^+ + r_N^{ss} f_{e,s}^- + r_N^{s\bar{s}} f_{e,\bar{s}}^- + r_A^{ss} f_{h,s}^+ + r_A^{s\bar{s}} f_{h,\bar{s}}^+, \tag{6}$$

$$\Psi_{ISC} = t_N^{ss} g_{e,s}^+ + t_N^{s\bar{s}} g_{e,\bar{s}}^+ + t_A^{ss} g_{h,s}^- + t_A^{s\bar{s}} g_{h,\bar{s}}^-, \tag{7}$$

with $\bar{s} = -s$. The coefficients $r_N^{ss(\bar{s})}$ and $r_A^{ss(\bar{s})}$ (or $t_N^{ss(\bar{s})}$ and $t_A^{ss(\bar{s})}$) are the reflection coefficients (or transmission coefficients) for the electron and the hole, respectively. The functions $f_{e,s(\bar{s})}$ and $f_{h,s(\bar{s})}$ (or $g_{e,s(\bar{s})}$ and $g_{h,s(\bar{s})}$) are the eigenvectors describing electron and hole with spin s ($\bar{s}$) in the FM region (or ISC region), respectively.[32,34] Based on the boundary conditions

$$\Psi_{FM}|_{x=0} = \Psi_{ISC}|_{x=0}, \quad \Psi'_{FM}|_{x=0} = \Psi'_{ISC}|_{x=0}, \tag{8}$$

we can obtain two AR probabilities

$$R_A^{ss} = \mathrm{Re}\left(\frac{q_{h,s}}{q_{e,s}}\right)|r_A^{ss}|^2, \quad R_A^{s\bar{s}} = \mathrm{Re}\left(\frac{q_{h,\bar{s}}}{q_{e,s}}\right)|r_A^{s\bar{s}}|^2, \tag{9}$$

where $q_{e,s}$ and $q_{h,s(\bar{s})}$ are the longitudinal wavevectors of the electron and hole states in the FM region. When an electron with spin s from one valley moves to the FM/ISC interface, as shown in Fig. 1(b), $R_A^{s\bar{s}}$ represents the normal AR for the reflected hole with opposite spin $\bar{s}$, while R_A^{ss} represents the equal-spin AR with the same spin s due to the spin-triplet pairing in the ISC. Note that the incident electron and the reflected hole always belong to opposite valleys, because that the Cooper pair in the ISC always forms from two electrons with opposite valleys. Below, we will show that the feature of AR probability strongly depends on the valley degree of freedom due to the irradiation of the circularly polarized light.

3. Results and discussion

In this section, we will discuss the valley-dependent equal-spin AR, normal AR, and spin transport controlled by the light, the chemical potential, and the magnetization direction. The superconducting gap is fixed as $\Delta = 1.0$ meV. The exchange energy M and Ising SOC strength λ_s are set as $M = 30.0$ meV and $\lambda_s = 10.0$ meV for convenience. The symbol $R_{\eta s \Rightarrow \bar{\eta} s(\bar{s})}$ in the following represents the AR probability that an incident election with spin s near valley η is reflected as a hole with spin s ($\bar{s}$) near opposite valley $\bar{\eta} = -\eta$. The units of λ_v, E, μ_{FM}, and μ_{ISC} are meV.

First, we discuss the normal AR process when the magnetization vector is in the out-of-plane direction with the polar angle $\theta = 0$. All the AR probabilities are independent of the azimuthal angle φ, so we take $\varphi = 0$ below. Figure 2 shows the AR probabilities $R_{K\downarrow\Rightarrow K'\uparrow}$ and $R_{K\uparrow\Rightarrow K'\downarrow}$ as functions of the potential μ_{FM} and the light λ_v at $\theta = 0.0$, $E = 0.0$, and $\mu_{ISC} = 0.0$. It can be found that only the normal AR could occur and equal-spin AR does not exist, where the incident electron and reflected hole belong to opposite spins and opposite valleys, due to the Cooper pairs $|KK', \downarrow\uparrow\rangle$, $|KK', \uparrow\downarrow\rangle$ in the ISC being valley singlet with its z-direction spin component $S_z = 0$. $R_{K\downarrow\Rightarrow K'\uparrow}$ and $R_{K\uparrow\Rightarrow K'\downarrow}$ take place in different areas. Here $R_{K\downarrow\Rightarrow K'\uparrow}$ and $R_{K'\uparrow\Rightarrow K\downarrow}$ are equal and occur in the same area $\mu_{FM} > |\lambda_v - M|$ [see Fig. 2(a)]. In fact, considering an incident electron from $K\downarrow$ band with the incident energy in the superconducting gap, the

transport processes from FM into the ISC can not occur and only two reflection processes (the normal reflection $R^N_{K\downarrow\Rightarrow K\downarrow}$ and normal AR $R_{K\downarrow\Rightarrow K'\uparrow}$) occur with $R^N_{K\downarrow\Rightarrow K\downarrow}+R_{K\downarrow\Rightarrow K'\uparrow}=1$. Similarly, for the incident particle from $K'\uparrow$ band, we have $R^N_{K'\uparrow\Rightarrow K'\uparrow}+R_{K'\uparrow\Rightarrow K\downarrow}=1$. The above four reflection processes form the scattering matrix $\begin{pmatrix} R^N_{K\downarrow\Rightarrow K\downarrow} & R_{K'\uparrow\Rightarrow K\downarrow} \\ R_{K\downarrow\Rightarrow K'\uparrow} & R^N_{K'\uparrow\Rightarrow K'\uparrow} \end{pmatrix}$ with $R^N_{K\downarrow\Rightarrow K\downarrow}+R_{K'\uparrow\Rightarrow K\downarrow}=R_{K\downarrow\Rightarrow K'\uparrow}+R^N_{K'\uparrow\Rightarrow K'\uparrow}=1$. Consequently, the two AR probabilities $R_{K\downarrow\Rightarrow K'\uparrow}$ and $R_{K'\uparrow\Rightarrow K\downarrow}$ are equal. In like manner, $R_{K\uparrow\Rightarrow K'\downarrow}=R_{K'\downarrow\Rightarrow K\uparrow}$ appears in the area $\mu_{\rm FM}>|\lambda_{\rm v}+M|$ [see Fig. 2(b)]. There is no AR in other areas because of the absence of incident electron mode or/and reflected hole mode. In addition, when the Ising superconducting phase is single band at $\mu_{\rm ISC}=0<\lambda_{\rm s}$, the Cooper pairs are mainly composed of $|K\downarrow\rangle$ and $|K'\uparrow\rangle$ electrons,[31,34] so $R_{K\uparrow\Rightarrow K'\downarrow}$ is very small compared with $R_{K\downarrow\Rightarrow K'\uparrow}$ [see the scale of the color bar in Figs. 2(a) and 2(b)].

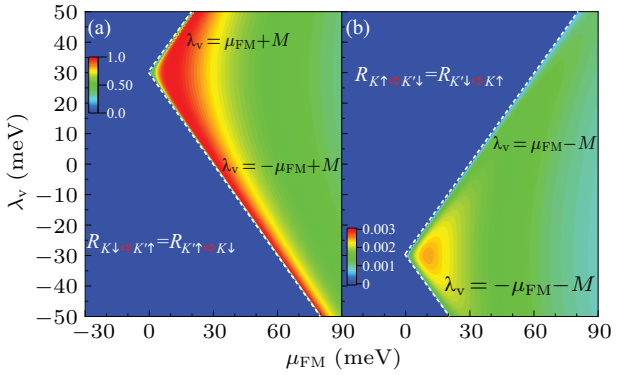


Fig. 2. AR probabilities (a) $R_{K\downarrow\Rightarrow K'\uparrow}$ and (b) $R_{K\uparrow\Rightarrow K'\downarrow}$ versus potential $\mu_{\rm FM}$ and light $\lambda_{\rm v}$ at $\theta=0.0$, $E=0.0$, and $\mu_{\rm ISC}=0.0$. The boundaries of AR probability are labelled by the dash curves $\lambda_{\rm v}=\pm\mu_{\rm FM}\pm M$, which are the critical values of the half-metal phase.

Next, we consider that the magnetization vector is in the in-plane direction with $\theta=\pi/2$ (i.e., in the x-direction). For the x-direction, both the spin-singlet and $S_x=\pm1$ spin-triplet Cooper pairs can exist in ISC. This is essentially different from the case of z-direction, where only $S_z=0$ Cooper pairs exist in ISC. Thus, the AR process would become intriguing. Figure 3 presents the AR probability as a function of the potential $\mu_{\rm FM}$ and the light $\lambda_{\rm v}$ when the electron injects from (a)–(d) K valley and (e)–(h) K' valley at $\theta=\pi/2$, $E=0.0$, and $\mu_{\rm ISC}=0.0$. Interestingly, the equal-spin AR appears due to the $S_x=\pm1$ spin-triplet Cooper pairs $|KK',\rightrightarrows\rangle$, $|KK',\leftleftarrows\rangle$ [see Figs. 3(b), 3(c), 3(f) and 3(g)]. In the equal-spin AR process, the incident electron and reflected hole possess the same spins but opposite valleys. The normal AR still survives [see Figs. 3(a), 3(d), 3(e) and 3(h)]. The equal-spin AR and normal AR include eight kinds of AR processes, which exhibit some interesting features.

(1) Various AR processes occur in different areas, depending on the spin and valley related band structure controlled by the potential $\mu_{\rm FM}$ and the light $\lambda_{\rm v}$. Compared to the normal AR, the equal-spin AR probability $R_{K(K')\rightarrow\Rightarrow K'(K)\rightarrow}$ occurs in a wider area [see Figs. 3(b) and 3(f)], while $R_{K(K')\leftarrow\Rightarrow K'(K)\leftarrow}$ occurs in a narrower area [see Figs. 3(c) and 3(g)], which can be changed by adjusting the magnetization and the light.

(2) Contrary to the situation at $\theta=0$ in Fig. 2, the normal AR probabilities $R_{K\rightarrow\Rightarrow K'\leftarrow}$ and $R_{K'\leftarrow\Rightarrow K\rightarrow}$ ($R_{K\leftarrow\Rightarrow K'\rightarrow}$ and $R_{K'\rightarrow\Rightarrow K\leftarrow}$) are no longer the same at $\theta=\pi/2$, as shown in Figs. 3(a) and 3(h) [Figs. 3(d) and 3(e)]. The reason is that for an incident electron with its spin in the x-direction, the four reflection processes (the normal reflection, the spin-flip reflection, the normal AR, and the equal-spin AR) occur at the FM/ISC interface, leading to that the scattering matrix is 4×4 and the matrix elements (various reflection probabilities) are in principle mutually unequal.

(3) In the presence of the light, the equal-spin AR and normal AR become sensitive to the valley degree of freedom. Due to the influence of the left and the right circularly polarized light on the character of the two valleys, the Hamiltonians between the two valleys satisfy

$$H_\eta(\lambda_{\rm v})=H_{\bar\eta}(-\lambda_{\rm v}) \tag{10}$$

in the FM lead. Thus, the AR near the two valleys are symmetric with respect to $\lambda_{\rm v}=0$, i.e.,

$$R_{\eta s\Rightarrow\bar\eta s(\bar s)}(\lambda_{\rm v})=R_{\bar\eta s\Rightarrow\eta s(\bar s)}(-\lambda_{\rm v}), \tag{11}$$

such as the AR probabilities $R_{K\rightarrow\Rightarrow K'\leftarrow}$ and $R_{K'\rightarrow\Rightarrow K\leftarrow}$ [see Figs. 3(a) and 3(e)].

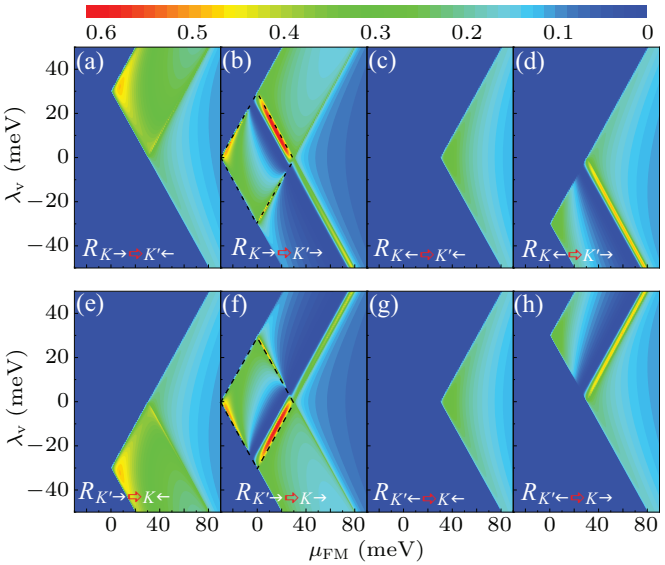


Fig. 3. AR probability versus potential $\mu_{\rm FM}$ and light $\lambda_{\rm v}$ for the incident electron from (a)–(d) K valley and (e)–(h) K' valley, at $\theta=\pi/2$, $E=0.0$, and $\mu_{\rm ISC}=0.0$.

(4) Importantly, there exists a special area where only the equal-spin AR probabilities $R_{K\rightarrow\Rightarrow K'\rightarrow}$ and $R_{K'\rightarrow\Rightarrow K\rightarrow}$ could take place while other AR processes are completely suppressed [see the rhombic area encircled by the black dashed

curves $\lambda_v = \pm\mu_{FM} \pm M$ in Figs. 3(b) and 3(f)], which could give rise to a spin supercurrent in ISC, as discussed in Fig. 7 in the following.

In order to see clearly the characters of AR, we plot the truncated intersection curves of AR probability as a function of (a) the light λ_v and (b) the potential μ_{FM} in Fig. 4. Figure 4(a) shows the symmetry between two certain AR processes around $\lambda_v = 0$. The AR appears in different regions of λ_v. The normal AR probabilities $R_{K\to\Rightarrow K'\leftarrow}$ and $R_{K'\leftarrow\Rightarrow K\to}$ are finite in the region $-\mu_{FM}+M < \lambda_v < \mu_{FM}+M$, while $R_{K\leftarrow\Rightarrow K'\to}$ and $R_{K'\to\Rightarrow K\leftarrow}$ have finite value in the region $-\mu_{FM}-M < \lambda_v < \mu_{FM}-M$. The equal-spin AR probabilities $R_{K\to\Rightarrow K'\to}$ and $R_{K'\to\Rightarrow K\to}$ occur in a broad region $-\mu_{FM}-M < \lambda_v < \mu_{FM}+M$. As shown in Fig. 4(b), the AR probability as a function of μ_{FM} could be divided into four regions, depending on the spin and valley related energy band in the FM region. There is no AR in the region $\mu_{FM} < -M+\lambda_v$, since the ISC is single-band phase and the FM region has no incident electron mode or/and no reflected hole mode at such a low chemical potential μ_{FM}. Only equal-spin AR probabilities $R_{K\to\Rightarrow K'\to}$ and $R_{K'\to\Rightarrow K\to}$ are nonzero in the region $-M+\lambda_v < \mu_{FM} < M-\lambda_v$, because only $S_x = 1$ spin-triplet and valley-singlet Cooper pairs $|KK',\rightrightarrows\rangle$ could be formed in ISC. Two equal-spin AR and two normal AR appear in the region $M-\lambda_v < \mu_{FM} < M+\lambda_v$ due to the existence of Cooper pairs $|KK',\rightrightarrows\rangle$ and $|KK',\rightleftarrows\rangle$. All of the eight AR can take place and all kinds of Cooper pairs can be formed in the region $\mu_{FM} > M+\lambda_v$.

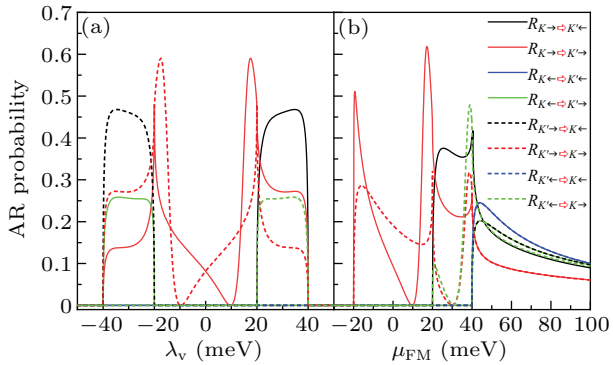


Fig. 4. AR probability versus (a) λ_v at $\mu_{FM} = 10.0$ meV and (b) μ_{FM} at $\lambda_v = 10.0$ meV. The values of the other parameters are the same as those in Fig. 3.

Figure 5 presents the AR probability as a function of incident energy E at $\theta = \pi/2$ and $\mu_{FM} = 50.0$ meV. When $\lambda_v = 0$ in Fig. 5(a), the two valleys in the FM region are degenerate, and so the AR process is independent of valley, that is $R_{\eta s\Rightarrow\bar{\eta}s(\bar{s})} = R_{\bar{\eta}s\Rightarrow\eta s(\bar{s})}$. The finite λ_v may break the degeneracy of the valley, leading to the valley-dependent AR [see Fig. 5(b)]. All the AR probabilities increase slightly with the incident energy in the subgap energy $E < \Delta$. When $\mu_{ISC} = 15.0$ meV $> \lambda_s$, the Ising superconducting phase changes to double-band from single-band, and so the normal AR is increased by the spin-singlet Cooper pairs [comparing Figs. 5(a) and 5(c)]. However, the equal-spin AR is decreased, since the spin-triplet pairing is rather weak for double-band ISC.[26,31] Out of subgap energy region $E > \Delta$, the normal AR probability decreases rapidly from a large value with the increase of the energy, regardless of the values of λ_v and μ_{ISC}. On the other hand, the equal-spin AR probability increases first from zero, then decreases slowly with the increase of the energy E from Δ. In addition, both normal AR and equal-spin AR present the resonant behavior near the superconducting gap edges, similar to the AR in N/SC junctions.[46] Particularly, the resonant normal AR exhibits a simple peak near $E = \Delta$, while the resonant equal-spin AR exhibits a peak followed by a dip.

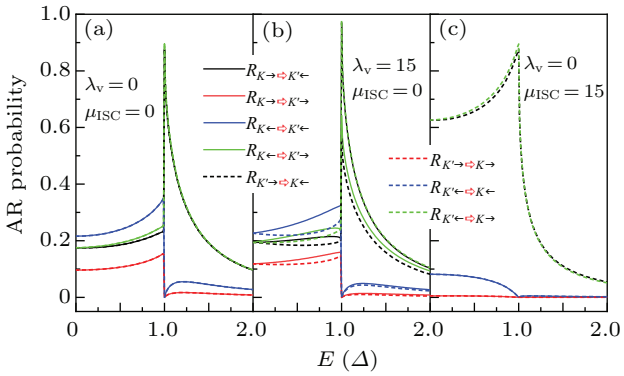


Fig. 5. AR probability versus the incident energy E at $\theta = \pi/2$ and $\mu_{FM} = 50.0$ meV.

The influence of off-resonant polarized light on the magnetoanisotropy of AR is discussed in Fig. 6. The AR probabilities for the incident electron from K and K' valleys are defined as

$$R_K = \Sigma_{s,\bar{s}} R_{Ks\Rightarrow K's(\bar{s})}, \quad R_{K'} = \Sigma_{s,\bar{s}} R_{K's\Rightarrow Ks(\bar{s})}. \tag{12}$$

The total AR probability is $R_K + R_{K'}$. In the presence of magnetization vector, the Hamiltonian H_η has the relation $\sigma_z H_\eta(\theta)\sigma_z^{-1} = H_\eta(-\theta)$, so $R_\eta(-\theta) = R_\eta(\theta)$, i.e., $R_K(\theta)$ and $R_{K'}(\theta)$ are symmetric about $\theta = 0$, as shown in Figs. 6(a) and 6(b). In the absence of the light with $\lambda_v = 0.0$, both AR probabilities R_K and $R_{K'}$ are anisotropic with respect to the magnetization direction θ, as shown in Fig. 6(a). R_K mainly appears in the third and fourth quadrants, while $R_{K'}$ mainly occurs in the first and second quadrants. The Hamiltonians between the two valleys can be related by the spin rotation operator σ_x,

$$\sigma_x H_{K'}(\pi-\theta)\sigma_x^{-1} = H_K(\theta). \tag{13}$$

This indicates that the AR probabilities between the two valleys have the relation

$$R_{K'}(\pi-\theta) = R_K(\theta). \tag{14}$$

The R_K and $R_{K'}$ are symmetric about $\theta = \pi/2$. As a consequence, the total AR probability $R_K + R_{K'}$ is magnetoanisotropic with period π. In the half-metal phase with $\mu_{\rm FM} = 10$ meV $< M - \lambda_{\rm v}$, only the equal-spin AR can occur (see Fig. 3). When the magnetization vector $\boldsymbol{M}$ is in the z direction with $\theta = 0$, the equal-spin AR is prohibited, then the AR probabilities R_K and $R_{K'}$ are zero [see Fig. 6(a)]. With the increase of θ from 0, the equal-spin AR occurs and the AR probabilities appear. When the right circularly polarized light is applied with $\lambda_{\rm v} = 5.0$ meV in Fig. 6(b), the symmetric relation equations (13) and (14) between the two valleys are destroyed. R_K is decreased but $R_{K'}$ is increased by the right circularly polarized light, because K is the minority valley and K' is the majority valley in the FM lead. Oppositely, the left circularly polarized light would increase R_K and decrease $R_{K'}$. Thus, the magnetoanisotropy of the total AR probability $R_K + R_{K'}$ becomes remarkable and the period becomes 2π instead of π in the presence of the light.

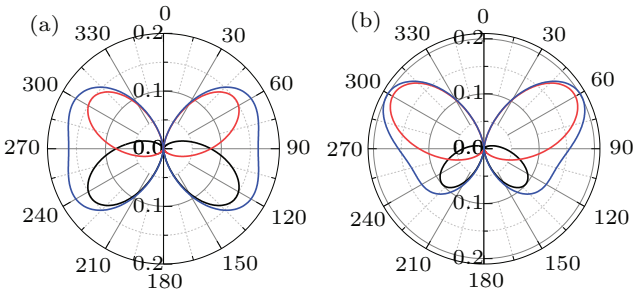


Fig. 6. AR probability versus the magnetization direction θ at (a) $\lambda_{\rm v} = 0.0$ and (b) $\lambda_{\rm v} = 5.0$ meV. The black, red, blue curves are for R_K, $R_{K'}$, and $R_K + R_{K'}$. Here, $\mu_{\rm FM} = 10.0$ meV, $E = 0.0$, and $\mu_{\rm ISC} = 0.0$.

Finally, we study the spin transport in this FM/ISC junction. As discussed in Figs. 3(b) and 3(f), only the equal-spin AR $R_{K\to\Rightarrow K'\to}$ and $R_{K'\to\Rightarrow K\to}$ could occur in the rhombic area. In this rhombic area, only the $S_x = 1$ spin-triplet Cooper pairs $|KK', \rightrightarrows\rangle$ are generated by the equal-spin AR processes and inject into ISC. There is no injection of the spin-singlet and other kinds of spin-triplet Cooper pairs. As a result, only the Cooper pairs $|KK', \rightrightarrows\rangle$ with spin $S = 1$ and $S_x = 1$ would flow along x direction in the ISC. This implies that a completely spin-polarized supercurrent appears in this rhombic area. If the direction of magnetization is inverted to $\theta = 3\pi/2$, the spin of the moving Cooper pairs would change to $S = 1$ and $S_x = -1$, and the Cooper pairs $|KK', \leftleftarrows\rangle$ would contribute to the charge current and the spin current. Observably, the direction of the spin-triplet Cooper pairs can be controlled by the magnetization and the light.

Considering the x-direction spin bias eV at the FM/ISC junction, the spin current I_s from FM lead flowing into ISC can be written as[35,47]

$$I_s = \frac{\hbar}{2}(J_\rightarrow - J_\leftarrow)$$
$$= \frac{1}{2}\int {\rm d}E \sum_{s=(\rightarrow,\leftarrow)} s\big[R_A^{ss}(f_{L,es} - f_{L,hs}) + R_N^{s\bar{s}}(f_{L,es} - f_{L,e\bar{s}}) + T_N^s(f_{L,es} - f_R)\big], \quad (15)$$

where R_A^{ss} is the equal-spin AR probability, $R_N^{s\bar{s}}$ is the spin-flip reflection probability, and T_N^s is the transmission probability. The spin index $s = \rightarrow, \leftarrow$ or $+, -$ in Eq. (15). The Fermi distribution function requires $f_{L,e\rightarrow} = f_{L,h\leftarrow} = f(E - eV)$ and $f_{L,e\leftarrow} = f_{L,h\rightarrow} = f(E + eV)$ in the FM lead and $f_R = f(E)$ in the ISC. The differential spin conductance can be obtained as $G_s = {\rm d}I_s/{\rm d}V$. The differential spin conductance for the incident electron from K (K') valley is labeled as $G_{s,K}$ ($G_{s,K'}$), satisfying $G_s = G_{s,K} + G_{s,K'}$. For the FM/ISC junction, the high spin injection efficiency occurs in the particular half-metal phase [e.g., in the rhombic area in Figs. 3(b) and 3(f)] where there is no spin-flip reflection.

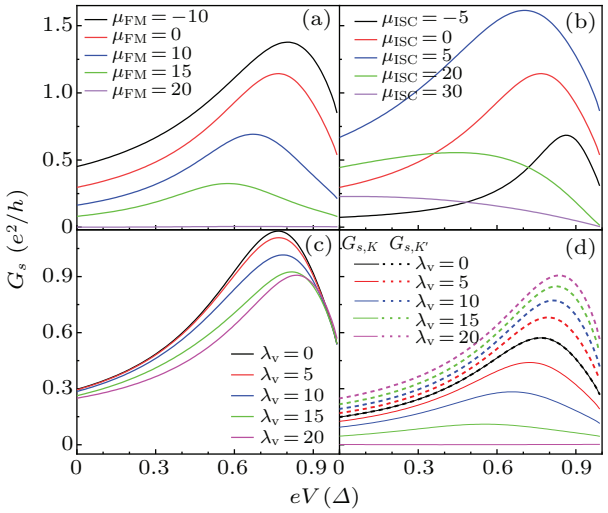


Fig. 7. Differential spin conductance G_s versus the finite spin bias eV at zero temperature for different values of (a) $\mu_{\rm FM}$, (b) $\mu_{\rm ISC}$, and (c) $\lambda_{\rm v}$. (d) $G_{s,K}$ and $G_{s,K'}$ versus eV for different values of $\lambda_{\rm v}$. The values of parameters are set as $\theta = \pi/2$, $\lambda_{\rm v} = 0.0$, $\mu_{\rm FM} = 0.0$, and $\mu_{\rm ISC} = 0.0$, unless otherwise noted in the figure.

Figure 7 displays the differential spin conductance as a function of finite spin bias eV with the parameters $\mu_{\rm FM}$ and $\lambda_{\rm v}$ in the rhombic area. Due to only the occurrence of the equal-spin AR in the rhombic area, the results are the same for the x-direction spin bias and the bias. From Fig. 7, one can see that with the continuous increase of spin bias, the differential spin conductance increases slowly at first, and then decreases rapidly after reaching its peak value. In the absence of light with $\lambda_{\rm v} = 0.0$, the differential spin conductance $G_{s,K}$ is the same as $G_{s,K'}$. The total G_s decreases with the increase of $\mu_{\rm FM}$ and tends to zero at $\mu_{\rm FM} = 20.0$ meV [see Fig. 7(a)]. As shown in Fig. 7(b), G_s increases gradually with $\mu_{\rm ISC}$ in the single-band superconducting phase (see the curves with $\mu_{\rm ISC} < \lambda_{\rm s}$). On the contrary, G_s decreases with $\mu_{\rm ISC}$ in the double-band superconducting phase (see the curves with $\mu_{\rm ISC} > \lambda_{\rm s}$). The reason is that the differential spin conductance

is mainly contributed by the equal-spin AR which mainly occurs in the single-band phase. With the appearance and increase of the light, G_s decreases relatively [see Fig. 7(c)]. Remarkably, the differential spin conductance $G_{s,K}$ is no longer equal to $G_{s,K'}$. It can be seen from Fig. 7(d) that as λ_v increases, $G_{s,K}$ decreases gradually but $G_{s,K'}$ increases gradually. At $\lambda_v = 20$ meV, only incident electrons from K' valley contribute to differential spin conductance. When the light changes from the right to the left circular polarization, $G_{s,K}$ will increase and $G_{s,K'}$ will decrease.

4. Conclusion

In summary, we studied the dependence of equal-spin AR on the valley degree of freedom in the light-irradiated FM/ISC junction based on Bogoliubov–de Gennes Hamiltonians. Due to the application of circularly polarized light, the properties of equal-spin AR and normal AR strongly depend on the valley degree of freedom. The resonant behavior of equal-spin AR near the superconducting gap edges is different from that of normal AR. The valley-dependent AR presents certain symmetry about light strength and magnetization angle, which can be understood by the symmetry of the system. The existence of $S_x = \pm 1$ spin-triplet Cooper pairs leads to a valley-dependent spin supercurrent in ISC which can be modulated by the light. Our results should be useful to the potential applications of ISC in spintronics and valleytronics.

Acknowledgements

Project supported by the National Natural Science Foundation of China (Grant Nos. 11974153, 12374034 and 11921005), the Innovation Program for Quantum Science and Technology (Grant No. 2021ZD0302403), and the Strategic Priority Research Program of Chinese Academy of Sciences (Grant No. XDB28000000).

References

[1] Schaibley J R, Yu H, Clark G, Rivera P, Ross J S, Seyler K L, Yao W and Xu X 2016 *Nat. Rev. Mater.* **1** 16055
[2] Zhao S, Li X, Dong B, Wang H, Wang H, Zhang Y, Han Z and Zhang H 2021 *Rep. Prog. Phys.* **84** 026401
[3] Sun J T and Meng S 2015 *Acta Phys. Sin.* **64** 187301 (in Chinese)
[4] Rycerz A, Tworzydło J and Beenakker C W J 2007 *Nat. Phys.* **3** 172
[5] Gorbachev R V, Song J C W, Yu G L, Kretinin A V, Withers F, Cao Y, Mishchenko A, Grigorieva I V, Novoselov K S, Levitov L S and Geim A K 2014 *Science* **346** 448
[6] Mak K F, McGill K L, Park J and McEuen P L 2014 *Science* **344** 1489
[7] Zhuang Y C and Sun Q F 2022 *Phys. Rev. B* **106** 165417
[8] Bertoni R, Nicholson C W, Waldecker L, Hübener H, Monney C, De Giovannini U, Puppin M, Hoesch M, Springate E, Chapman R T, Cacho C, Wolf M, Rubio A and Ernstorfer R 2016 *Phys. Rev. Lett.* **117** 277201
[9] Xiao D, Liu G B, Feng W, Xu X and Yao W 2012 *Phys. Rev. Lett.* **108** 196802
[10] Liu Y W, Hou Z, Li S Y, Sun Q F and He L 2020 *Phys. Rev. Lett.* **124** 166801
[11] Zubair M, Vasilopoulos P and Tahir M 2022 *Phys. Rev. B* **106** 205402
[12] Beenakker C W J 2008 *Rev. Mod. Phys.* **80** 1337
[13] Akhmerov A R and Beenakker C W J 2007 *Phys. Rev. Lett.* **98** 157003
[14] Linder J and Yokoyama T 2014 *Phys. Rev. B* **89** 020504(R)
[15] Majidi L and Asgari R 2014 *Phys. Rev. B* **90** 165440
[16] Schroer A, Silvestrov P G and Recher P 2015 *Phys. Rev. B* **92** 241404(R)
[17] Lu W T and Sun Q F 2021 *Phys. Rev. B* **104** 045418
[18] Qi F, Cao J and Jin G 2018 *Phys. Rev. B* **98** 045422
[19] Qi F, Cao J, Cao J and Zhang L 2018 *Chin. Phys. B* **27** 127401
[20] Yan Q, Zhou Y F and Sun Q F 2020 *Chin. Phys. B* **29** 097401
[21] Taniguchi K, Matsumoto A, Shimotani H and Takagi H 2012 *Appl. Phys. Lett.* **101** 042603
[22] Lu J M, Zheliuk O, Leermakers I, Yuan N F Q, Zeitler U, Law K T and Ye J T 2015 *Science* **350** 1353
[23] Xi X, Wang Z, Zhao W, Park J H, Law K T, Berger H, Forró L, Shan J and Mak K F 2016 *Nat. Phys.* **12** 139
[24] Costanzo D, Zhang H, Reddy B A, Berger H and Morpurgo A F 2018 *Nat. Nanotechnol.* **13** 483
[25] Hamill A, Heischmidt B, *et al.* 2021 *Nat. Phys.* **17** 949
[26] Zhou B T, Yuan N F Q, Jiang H L and Law K T 2016 *Phys. Rev. B* **93** 180501
[27] Lesser O, Shavit G and Oreg Y 2020 *Phys. Rev. Research* **2** 023254
[28] Xie Y, Zhou B T, Ng T K and Law K T 2020 *Phys. Rev. Research* **2** 013026
[29] Möckli D and Khodas M 2020 *Phys. Rev. B* **101** 014510
[30] Tang G, Bruder C and Belzig W 2021 *Phys. Rev. Lett.* **126** 237001
[31] Lv P, Zhou Y F, Yang N X and Sun Q F 2018 *Phys. Rev. B* **97** 144501
[32] Cheng Q and Sun Q F 2019 *Phys. Rev. B* **99** 184507
[33] Tang G, Klees R L, Bruder C and Belzig W 2021 *Phys. Rev. B* **104** L241413
[34] Lu W T, Sun Q F and Cheng Q 2022 *Phys. Rev. B* **105** 125425
[35] Dai Y X, Mao Y and Sun Q F 2022 *Phys. Rev. B* **106** 184513
[36] Fausti D, Tobey R I, Dean N, Kaiser S, Dienst A, Hoffmann M C, Pyon S, Takayama T, Takagi H and Cavalleri A 2011 *Science* **331** 189
[37] Mitrano M, Cantaluppi A, Nicoletti D, Kaiser S, Perucchi A, Lupi S, Di Pietro P, Pontiroli D, Riccò M, Clark S R, Jaksch D and Cavalleri A 2016 *Nature* **530** 461
[38] Liu M, Hwang H Y, Tao H, Strikwerda A C, Fan K, Keiser G R, Sternbach A J, West K G, Kittiwatanakul S, Lu J, Wolf S A, Omenetto F G, Zhang X, Nelson K A and Averitt R D 2012 *Nature* **487** 345
[39] Sentef M A, Claassen M, Kemper A F, Moritz B, Oka T, Freericks J K and Devereaux T P 2015 *Nat. Commun.* **6** 7047
[40] Hubener H, Sentef M A, De Giovannini U, Kemper A F and Rubio A 2017 *Nat. Commun.* **8** 13940
[41] Mclver J W, Schulte B, Stein F U, Matsuyama T, Jotzu G, Meier G and Cavalleri A 2020 *Nat. Phys.* **16** 38
[42] Kitagawa T, Oka T, Brataas A, Fu L and Demler E 2011 *Phys. Rev. B* **84** 235108
[43] Platero G and Aguado R 2004 *Phys. Rep.* **395** 1
[44] Ezawa M 2013 *Phys. Rev. Lett.* **110** 026603
[45] Tahir M, Manchon A and Schwingenschlögl U 2014 *Phys. Rev. B* **90** 125438
[46] Blonder G E, Tinkham M and Klapwijk T M 1982 *Phys. Rev. B* **25** 4515
[47] Sun Q F and Xie X C 2009 *J. Phys.: Condens. Matter* **21** 344204